EARTHQUAKE ENGINEERING AND STRUCTURAL DYNAMICS
Earthquake Engng Struct. Dyn. 2000; **29**: 1375–1404

Linear dynamic modeling of a uni-axial servo-hydraulic shaking table system

J. P. Conte[1,*,†,‡] and T. L. Trombetti[2,§]

[1]*Department of Civil and Environmental Engineering, University of California, Los Angeles, California 90095-1593, U.S.A.*
[2]*Dipartimento D.I.S.T.A.R.T., Facolta di Ingegneria, Universita degli Studi di Bologna, viale Risorgimento 2, 40136 Bologna, Italy*

SUMMARY

This paper focuses on the development of a linear analytical model (even though servo-hydraulic actuation systems are inherently non-linear, especially for large amplitude simulations — near the performance capacity of the system — linearized models proved experimentally to be quite effective overall in capturing the salient features of shaking table dynamics) of a uni-axial, servo-hydraulic, stroke controlled shaking table system by using jointly structural dynamics and linear control theory. This model incorporates the proportional, integral, derivative, feed-forward, and differential pressure gains of the control system. Furthermore, it accounts for the following physical characteristics of the system: time delay in the servovalve response, compressibility of the actuator fluid, oil leakage through the actuator seals and the dynamic properties of both the actuator reaction mass and test structure or payload. The proposed model, in the form of the total shaking table transfer function (i.e. between commanded and actual table motions), is developed to account for the specific characteristics of the Rice University shaking table. An in-depth sensitivity study is then performed to determine the effects of the table control parameters, payload characteristics, and servovalve time delay upon the total shaking table transfer function. The sensitivity results reveal: (a) a potential strong dynamic interaction between the oil column in the actuator and the payload, and (b) the very important effect of the servovalve time delay upon the total shaking table transfer function. Copyright © 2000 John Wiley & Sons, Ltd.

KEY WORDS: servo-hydraulic shaking table system; stroke control; servovalve time delay; servovalve–actuator–foundation–specimen interaction; PID, feed-forward and differential pressure control; shaking table transfer function

* Correspondence to: J. P. Conte, Department of Civil and Environmental Engineering, University of California, 5731G Boelter Hall, Los Angeles, CA 90095-1593, U.S.A.
† Associate Professor, formerly at Rice University, Houston, Texas 77251, U.S.A.
‡ E-mail: jpconte@seas.ucla.edu.
§ Assistant Professor, formerly Graduate Student at Rice University, Houston, Texas, U.S.A.

Contract/grant sponsor: National Science Foundation, Rice University.
Contract/grant number: BCS-9311031.

Received 23 September 1999
Revised 13 March 2000
Accepted 28 March 2000

1. INTRODUCTION

The main objective of a shaking table system is the high-fidelity reproduction of displacement or acceleration time histories such as earthquake accelerograms. However, reproduction of a dynamic signal is known to remain imperfect [1–3]. The degree of distortion in signal reproduction depends on numerous factors such as physical system parameters (e.g. foundation compliance, compressibility of oil column in the actuator chamber, oil leakage through the actuator seals, non-linear flow characteristics in the actuator, servovalve time delay, etc.), configuration and characteristics of control loop(s) (e.g. type of control algorithm, feedback signals, dynamics of sensors measuring the feedback response quantities, signal conditioning, characteristics of the digital data acquisition and control system — A/D and D/A boards, anti-aliasing filters, … — control gain setting, etc.), and characteristics of the test structure. To fully understand and exploit the actual testing capabilities of a shaking table, a mere evaluation of the accuracy of the table in reproducing base motions is not sufficient. A complete study of the table sensitivities with respect to all pertinent system and payload parameters is necessary in order to optimize the physical parameters and the control gain settings for maximum accuracy in motion reproduction by the table under a range of payload conditions. Furthermore, a thorough understanding of the table–payload dynamic interaction is essential for thoughtful design and proper results interpretation of shaking table experiments.

The paper first presents the development of a linear analytical dynamic model of a uni-axial, stroke (displacement) controlled shaking table system in the form of the total shaking table transfer function (in Laplace domain) between desired (or commanded) and actual table motions. The present model was arrived at by progressively incorporating physical and control characteristics until it was capable of predicting well the observed dynamic performance of the Rice University shaking table for a wide range of operating conditions [4, 5]. The analytical model developed accounts specifically for proportional, integral, derivative, feed-forward, and differential pressure control gains, as well as the effects of actuator oil compressibility, oil leakage across the sealed joints within the actuator, time delay in the response of the servovalve spool to a given electrical signal, compliance of the actuator reaction mass, and dynamic characteristics of the test structure (or payload) modeled as linear elastic SDOF and 2-D MDOF systems. As the Rice University earthquake simulator is controlled by a digitally supervised analog controller, the present model does not account for phenomena related to signal digitization. Sensor (LVDT and pressure transducers) dynamics are not considered here since they are insignificant in the operating frequency range (0–80 Hz) of the Rice shaking table. For the same reason, the analog low-pass filters applied to the displacement and delta-pressure feedback signals are ignored. Second, the paper presents selective results of the sensitivity analysis of the total shaking table transfer function with respect to table control parameters, payload dynamic characteristics, and servovalve time delay.

2. ANALYTICAL MODELLING OF SHAKING TABLE SYSTEM

This section presents the development, from basic principles, of a linear analytical model able to capture the salient dynamic characteristics of a servo-hydraulic, stroke-controlled, uni-axial shaking table system. The objective of this analytical model is to represent mathematically the

input–output relationship between desired (or commanded) and actual absolute[†] table motions. For openness of the model to possible further extensions and facilitation of its physical understanding, the model is developed following the modular approach depicted in Figure 1 and described below. This approach breaks down the shaking table system into several subsystems.

(1) First, a linearized analytical model for the 'Three-Stage Servovalve Transfer Function', $H_t(s)$, is developed. It is then used in conjunction with the flow continuity equation in the actuator to yield the 'Servovalve–Actuator Transfer Function', $S(s)$.
(2) Second, the servovalve–actuator model is incorporated into the analytical model for the controller (outer table control loop) giving rise to the so-called 'Servo-Hydraulic System Transfer Function', $H(s)$.
(3) Third, the effects of the flexibility (or compliance) of the actuator reaction mass are accounted for through the so-called 'Base Transfer Function' $B(s)$, leading to an expression for the 'Shaking Table Transfer Function', $T(s)$, between desired and actual table motions.
(4) Lastly, the effects of the test structure (both SDOF and MDOF) dynamic characteristics, modeled through the so-called 'Payload Transfer Function', $H_p(s)$, are taken into consideration. The presence of a test structure on the shaking table modifies the expression for $S(s)$, $H(s)$, and $B(s)$, thus giving a modified expression for the shaking table transfer function $T(s)$.

2.1. Three-stage servovalve transfer function, $H_t(s)$

The functioning of a three-stage servovalve characterized by an 'inner feedback control loop' is represented schematically in Figure 2.[‡] In this paper, the three-stage servovalve transfer function, $H_t(s)$, is defined as the ratio between the oil flow rate, $q_s(s)$, provided by the third-stage of the servovalve to the actuator pressure chamber[§] and the electrical command signal[¶] to the servovalve, $x_c(s)$:

$$H_t(s) = \frac{q_s(s)}{x_c(s)} \tag{1}$$

The Laplace notation is used throughout the paper. Referring to Figure 2, the functioning of the three-stage servovalve can be summarized as follows. The servovalve command signal, $x_c(s)$, before being sent to the electric coil which moves the flapper (i.e. the first stage of the servovalve), is processed by the controller through the so-called 'inner control loop' in order to yield the inner loop conditioned servovalve command signal, $x_{ci}(s)$. The electric signal, $x_{ci}(s)$, controls the rotation of the pilot flapper which generates a differential pressure in the pilot stage (or second stage), $\Delta P_P(s)$. The differential pressure $\Delta P_P(s)$ thus created controls the position of the second-stage spool (or pilot spool) which in turn controls the flow of hydraulic fluid into the third stage and the position of the third-stage spool, $x_{3s}(s)$. Finally the position of the third-stage spool,

[†] With respect to an inertial reference frame.
[‡] In this diagram the signal corresponding to the dither motion (used in servovalves in order to prevent any stick–slip behaviour of the moving components) has been ignored, since the high frequency at which the dither motion operates (500 Hz) is far out of the operational frequency range (0–80 Hz) of the servovalve and actuator.
[§] Actuator chamber on the pressure side of the piston, see Figure 3.
[¶] Conditioned by the outer control loop, but unconditioned by the inner control loop.

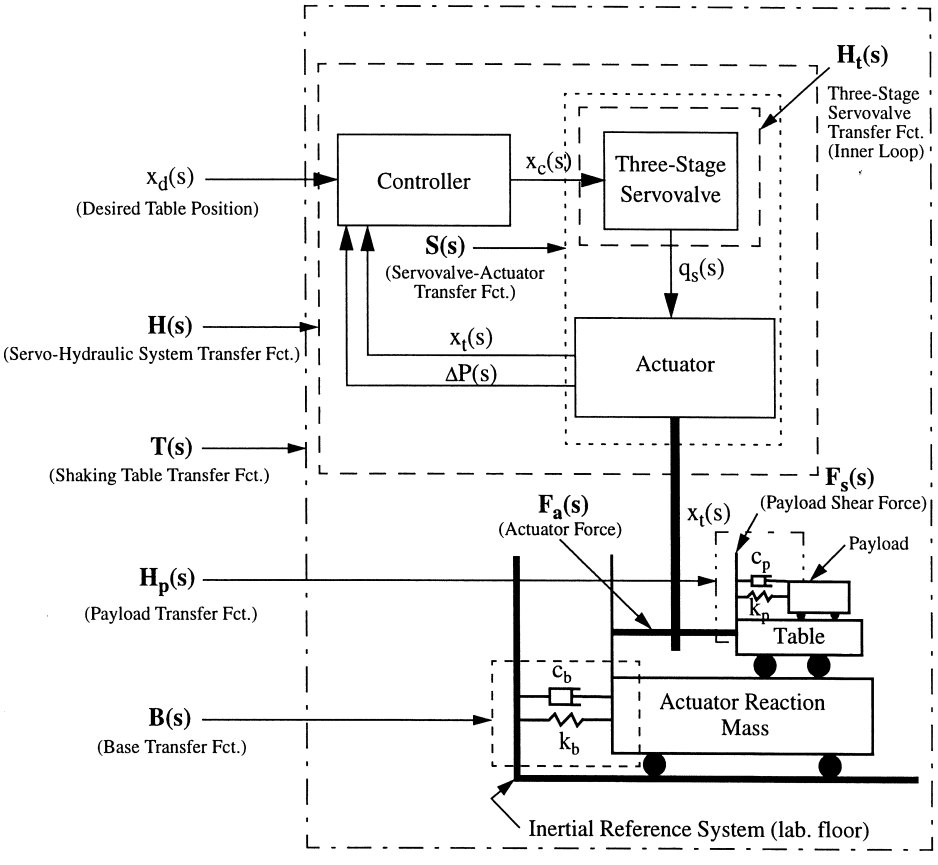

Figure 1. Block diagram of shaking table system.

$x_{3s}(s)$, controls the flow of high-pressure hydraulic fluid into the actuator pressure chamber, $q_s(s)$. As already suggested by previous investigators [1, 3, 6] linear relationships are assumed between: (a) the inner loop conditioned servovalve command, $x_{ci}(s)$, and the pilot stage differential pressure, $\Delta P_P(s)$, (b) the pressure drop induced across the pilot stage spool, $\Delta P_P(s)$, and the displacement of the main stage spool, $x_{3s}(s)$, and (c) the main stage spool position, $x_{3s}(s)$, and the fluid flow rate into the actuator pressure chamber, $q_s(s)$. These linear assumptions together with the proportional-derivative inner control loop lead to the following three-stage servovalve transfer function:

$$H_t(s) = \frac{q_s(s)}{x_c(s)} = k_{xq} \frac{k_1 k_2 (K^i_{pro} + sK^i_{der})}{1 + A_i(s) k_1 k_2 (K^i_{pro} + sK^i_{der})} \tag{2}$$

in which k_1 is the flapper gain, $\Delta P_p(s) = k_1 x_{ci}(s)$, k_2 is the second-stage gain factor, $x_{3s}(s) = k_2 \Delta P_p(s)$, k_{xq} is the flow-gain coefficient, $q_s(s) = k_{xq} x_{3s}(s)$, K^i_{pro} is the inner loop proportional gain

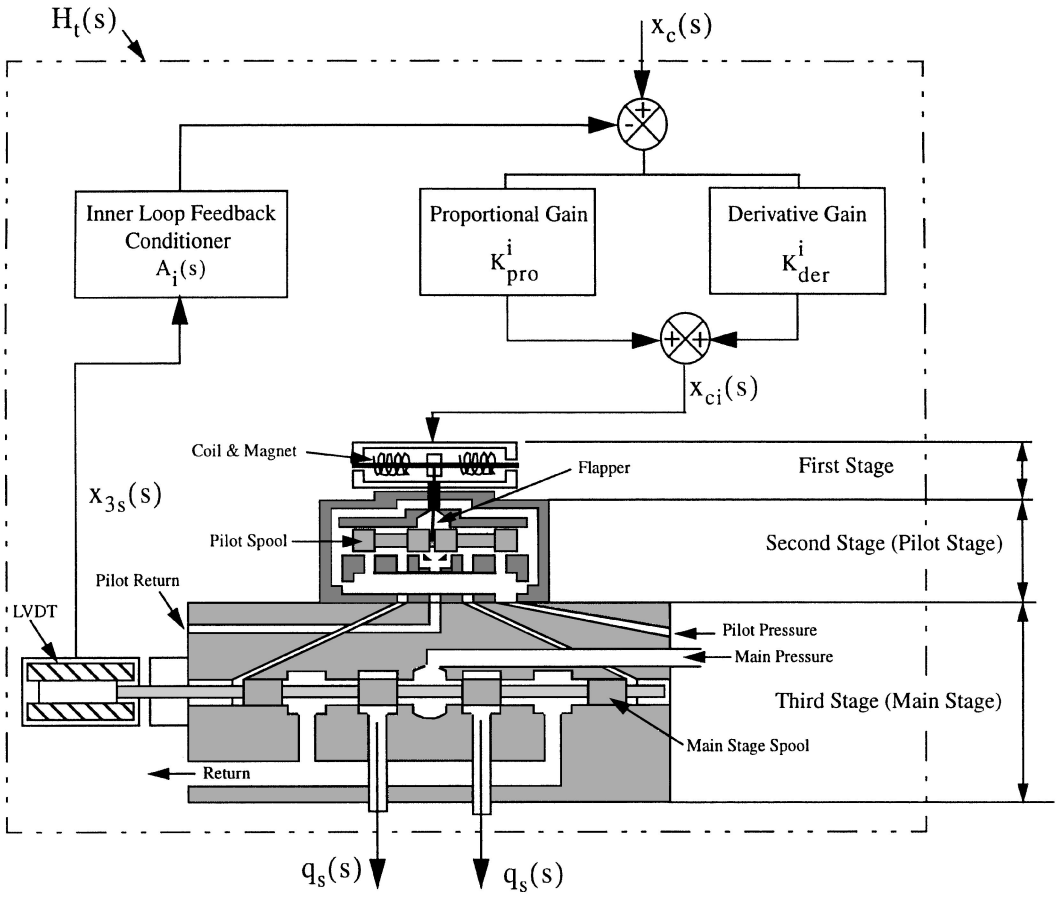

Figure 2. Three-stage servovalve functioning.

constant, K^i_{der} is the inner loop derivative gain constant, and $A_i(s)$ is the so-called 'inner loop' feedback transfer function (or feedback conditioner) which, in most cases, is set to unity.

As the servovalve can be driven much more accurately than the remainder of the shaking table system (actuator, outer control loop, reaction mass), the effect of the inner control loop is usually neglected in shaking table modeling [1, 3]. This can be achieved by setting $K^i_{pro} = 1$ v/v, $K^i_{der} = A_i(s) = 0$, thus leading to the following simplified expression for the three-stage servovalve transfer function:

$$H_t(s) = \frac{q_s(s)}{x_c(s)} = k_2 k_1 k_{xq} = k_t \tag{3}$$

in which $k_t = k_{xq} k_1 k_2$ is termed the table gain factor. It is worth mentioning that the servovalve models in Equations (2) and (3), although widely used, may in certain cases not be sufficient to predict accurately the shaking table behaviour. An effective improvement of these servovalve

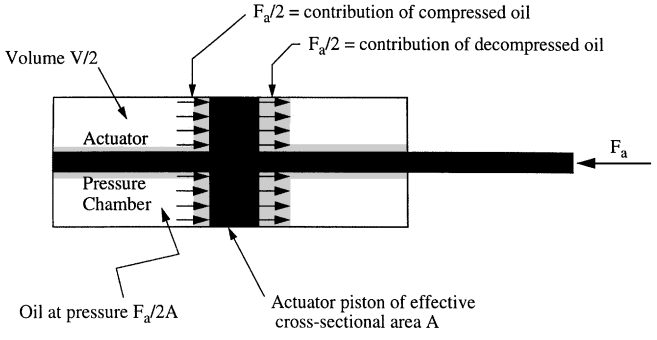

Figure 3. Oil flow to compensate for oil compressibility.

models can be obtained by introducing a time delay τ between the instant at which the electrical signal $x_{ci}(t)$ reaches the first stage of the servovalve and the instant at which the third-stage spool has responded correspondingly†. This time delay can be physically interpreted as the time necessary to overcome the mechanical and hydraulic inertia of the servovalve. Thus,

$$x_{3s}(t) = k_1 k_2 x_{ci}(t - \tau) \tag{4}$$

or, in Laplace notation

$$x_{3s}(s) = k_1 k_2 x_{ci}(s) e^{-\tau s}$$

This improvement modifies the servovalve transfer functions in Equations (2) and (3) as, respectively,

$$H_t(s) = \frac{q_s(s)}{x_c(s)} = k_{xq} \frac{k_1 k_2 (K^i_{pro} + sK^i_{der})}{1 + A_i(s) k_1 k_2 (K^i_{pro} + sK^i_{der}) e^{-\tau s}} e^{-\tau s} \tag{5}$$

$$H_t(s) = \frac{q_s(s)}{x_c(s)} = k_t e^{-\tau s} \tag{6}$$

2.2. *Servovalve–actuator transfer function, S(s)*

The high-pressure hydraulic fluid flow rate delivered through the servovalve, $q_s(t)$, ports into the actuator pressure chamber. This fluid flow rate must compensate for (a) the change in volume (per unit time) of the actuator pressure chamber, $q_{pm}(s)$, due to the actuator piston motion, (b) the flow rate of fluid leaking through the actuator seals, $q_{le}(s)$, and (c) the compressibility of the oil in the

† The existence of a time delay in the servovalve response can be anticipated from basic dynamic considerations (inertia effects) and it was observed experimentally by the authors during tuning of the Rice University shaking table.

actuator pressure chamber, $q_{\text{comp}}(s)$. This leads to the following flow continuity equation in the actuator:

$$q_{\text{s}}(s) = q_{\text{pm}}(s) + q_{\text{le}}(s) + q_{\text{comp}}(s) \tag{7}$$

The fluid flow rate $q_{\text{pm}}(t)$ which compensates for the change in volume of the actuator pressure chamber can be expressed as $q_{\text{pm}}(t) = A\dot{x}_t(t)$ where $\dot{x}_t(t)$ is the velocity of the actuator arm (relative to the body of the actuator), and A is the effective cross-sectional area of the actuator piston.

Assuming a linear relationship [1, 3, 6] between the fluid leakage through the actuator seals and the pressure of the fluid in the actuator pressure chamber, the component of flow rate due to leakage, $q_{\text{le}}(t)$, can be related to the force acting across the actuator, $F_{\text{a}}(t)$, as

$$q_{\text{le}}(t) = k'_{\text{le}} \frac{F_{\text{a}}(t)}{A} = k_{\text{le}} F_{\text{a}}(t) \tag{8}$$

where k'_{le} is the flow-pressure coefficient (or 'valve leakage' [6]) expressing the linear relationship between the differential pressure across the actuator piston and the flow rate of leaking fluid, and $k_{\text{le}} = k'_{\text{le}}/A$ is the corresponding flow-force coefficient.

When the oil in the actuator pressure chamber is subjected to an external pressure, it undergoes a change in volume ΔV, due to its finite bulk modulus. The relationship between pressure change and change in volumetric strain for a fluid is given by

$$\Delta P_{\text{oil}} = \beta \frac{\Delta V}{V_{\text{ref}}} \tag{9}$$

where ΔP_{oil} is the pressure change in the fluid, β is the bulk modulus of the fluid, and V_{ref} is the reference volume of the fluid under consideration.

By considering the average piston position shown in Figure 3, the pressure change in the fluid of the actuator pressure chamber is equal to half the force applied through the actuator arm divided by the piston effective cross-sectional area, i.e., $\Delta P_{\text{oil}} = F_{\text{a}}(t)/2A$, and the reference volume of fluid under consideration is equal to half the total volume V of both chambers of the actuator, i.e., $V_{\text{ref}} = V/2$. Substituting the previous expressions for ΔP_{oil} and V_{ref} into Equation (9), we obtain the following expression for the total change in volume ΔV of the oil in the actuator pressure chamber due to oil compressibility:

$$\Delta V(t) = \frac{V}{4\beta} \frac{F_{\text{a}}(t)}{A} \tag{10}$$

The fluid flow rate due to oil compressibility is obtained by taking the time derivative of the above volume change, i.e.

$$q_{\text{comp}}(t) = \frac{\text{d}}{\text{d}t}[\Delta V(t)] = \frac{V}{4\beta A} \dot{F}_{\text{a}}(t) \tag{11}$$

Substituting the above three components of fluid flow rate into the flow continuity equation, Equation (7), we obtain the following expression for the oil flow rate from the servovalve into the

actuator pressure chamber

$$q_s(s) = sAx_t(s) + k_{le}F_a(s) + s\frac{V}{4\beta A}F_a(s) \tag{12}$$

Then, by combining Equations (1) and (12), we obtain the following expression for the servovalve–actuator transfer function, $S(s)$

$$S(s) = \frac{x_t(s)}{x_c(s)} = \frac{H_t(s)}{sA + k_{le}(F_a(s))/(x_t(s)) + s(V/4\beta A)(F_a(s))/(x_t(s))} \tag{13}$$

Note that, for the sake of modularity, the above servovalve–actuator transfer function is expressed in terms of the actuator force, $F_a(s)$, and actuator arm (relative) displacement, $x_t(s)$. Appropriate expressions for $F_a(s)$ and $x_t(s)$ are derived in the following sections.

2.3. Servo-hydraulic system transfer function, H(s)

Most controllers determine the servovalve electrical command signal $x_c(t)$ as a sum of different components

$$x_c(t) = \varepsilon(t) + x_{ff}(t) + x_{dp}(t) \tag{14}$$

where $\varepsilon(t)$ is an (electrical) component proportional to the table error (= difference between the table desired displacement, $x_d(t)$, and the actual displacement, $x_t(t)$, of the actuator arm[†]) conditioned through the PID control scheme;[‡] the feed-forward (electrical) component $x_{ff}(t)$ is proportional to the derivative of the desired displacement; and $x_{dp}(t)$ is an (electrical) component proportional to the differential pressure across the actuator piston (referred to as the delta pressure component). In Laplace notation, the PID conditioned table error component is given as

$$\varepsilon(s) = \left[K_{pro} + \frac{1}{s}K_{int} + sK_{der}\right][x_d(s) - x_t(s)] \tag{15}$$

in which K_{pro} is the proportional control gain; K_{int} is the integral control gain, and K_{der} is the derivative control gain.

The feed-forward (electrical) component, $x_{ff}(s)$, can be expressed as $x_{ff}(s) = sK_{ff}x_d(s)$ where K_{ff} is the feed-forward control gain. The differential pressure (electrical) component, $x_{dp}(s)$, can be expressed as $x_{dp}(s) = K_{dp}\Delta P(s)$ where K_{dp} is the delta pressure control gain,[§] and $\Delta P(s)$, the differential pressure across the actuator piston, can be expressed in terms of the force in the

[†] The position of the actuator arm is the same as the table's position assuming that they are rigidly coupled.

[‡] PID stands for proportional–integral–derivative control [7].

[§] In this paper, for the sake of clarity, the quantities x_d, x_t, ΔP, F_a, F_s are assumed to carry their original physical dimensions. The conversion factors from these physical dimensions (m (in), Pa (psi), N (lbs)) to the corresponding electrical signals (V) are assumed to be lumped with the control gain constants. For example, herein K_{pro} is in units of V/cm (V/in) while on the actual controller, the proportional gain P_{gain} is defined in (V/V) and is related to K_{pro} through the relation $K_{pro}(V/cm) = P_{gain}(V/V)K_{xt}(V/cm)$ where K_{xt} denotes the transfer function of the actuator arm LVDT (displacement feedback sensor) here adequately approximated as a constant.

actuator $F_a(s)$ as $\Delta P(s) = F_a(s)/A$. Substituting all the above expressions into Equation (14) yields the following expression for the servovalve electrical command signal $x_c(s)$:

$$x_c(s) = \left[K_{pro} + \frac{1}{s}K_{int} + sK_{der}\right][x_d(s) - x_t(s)] + sK_{ff}x_d(s) + K_{dp}\frac{F_a(s)}{A} \tag{16}$$

Substituting $x_c(s) = x_t(s)/S(s)$ from Equation (13) into Equation (16) yields the following useful general expression for the transfer function between the desired table displacement, $x_d(s)$, and the actual displacement (relative to the body of the actuator or top of the reaction mass), $x_t(s)$, of the actuator arm

$$H(s) = \frac{x_t(s)}{x_d(s)} = \frac{S(s)[(1/s)K_{int} + K_{pro} + s(K_{ff} + K_{der})]}{1 + S(s)[(1/s)K_{int} + K_{pro}) + sK_{der} - ((K_{dp}/A)(F_a(s)/x_t(s))]} \tag{17}$$

In this paper, $H(s)$ is referred to as the 'servo-hydraulic system transfer function'. It is worth mentioning that the table control parameters K_{pro}, K_{int}, K_{der}, K_{ff}, and K_{dp} are user-set gains on the controller.

2.4. Shaking table transfer function, T(s), including foundation compliance effects

In reality, the actuator reaction mass is not perfectly rigid and fixed with respect to an inertial reference system, but has some degree of flexibility (or compliance). As shown in Figure 4, the absolute shaking table displacement, $x_{ta}(t)$, with respect to an inertial reference system (lab. floor) is obtained simply as the sum of the displacement, $x_t(t)$, of the actuator arm relative to the reaction mass and the displacement of the reaction mass, $x_b(t)$, relative to the inertial reference system (lab. floor) as

$$x_{ta}(t) = x_t(t) + x_b(t) \tag{18}$$

The total shaking table transfer function defined as the transfer function between the desired absolute table displacement, $x_d(s)$, and the actual absolute table displacement response, $x_{ta}(s)$, thus takes the following expression:

$$T(s) = \frac{x_{ta}(s)}{x_d(s)} = \frac{x_b(s) + x_t(s)}{x_d(s)} = \frac{x_t(s)}{x_d(s)}\left(\frac{x_b(s)}{x_t(s)} + 1\right) = H'(s)(B(s) + 1) \tag{19}$$

in which $H'(s) = x_t(s)/x_d(s)$ is the servo-hydraulic system transfer function as obtained using the expression for the actuator force, $F_a(s)$, which takes into account the effects of reaction mass flexibility or foundation compliance;[†] and $B(s) = x_b(s)/x_t(s)$, referred to as the base transfer function, is defined as the transfer function between the relative displacement, $x_t(s)$, of the actuator arm and the displacement, $x_b(s)$, of the reaction mass relative to an inertial reference system (lab. floor).

[†] The reaction mass flexibility or foundation compliance affects the absolute motion of the slip table, the inertia forces generated by the slip table mass and, consequently, the force in the actuator $F_a(t)$.

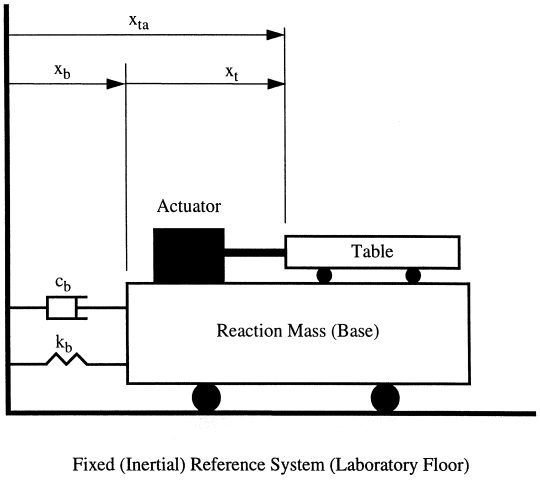

Figure 4. Coordinate system for shaking table and flexible base.

From the equation of motion of the actuator reaction mass (modeled herein as an SDOF system) subjected to the inertia force of the slip table accelerated by the actuator arm, it can be shown that

$$B(s) = \frac{x_b(s)}{x_t(s)} = -\frac{m_t}{m_T}\frac{s^2}{s^2 + s2\xi_b\omega_b + \omega_b^2} \tag{20}$$

where $m_T = m_b + m_t$ is the total mass of the system;[†] $\omega_b = \sqrt{k_b/m_T}$ and $\xi_b = c_b/(2\sqrt{k_b m_T})$ are the natural circular frequency and the damping ratio, respectively, of the reaction mass or flexible foundation. In the above, k_b represents the effective stiffness of the reaction mass. If the reaction mass is flexible internally, then m_b becomes an effective total mass instead of the exact total mass.

Assuming that no friction exists between the slip table and the rails, that the actuator damping is internal to the servovalve system and that the table is carrying no payload (i.e. bare table condition), the force in the actuator, $F_a(t)$, is equal to the slip table mass, m_t, multiplied by the slip table absolute acceleration.[‡] Thus

$$F_a(s) = s^2 m_t x_{ta}(s) = s^2 m_t x_t(s)\left[1 + \frac{x_b(s)}{x_t(s)}\right] = x_t(s)s^2 m_t[1 + B(s)] \tag{21}$$

[†] Total mass of the system $m_T = m_b + m_t$ where m_b denotes the reaction mass (including the mass of the fixed parts of the servovalve–actuator system) and m_t denotes the mass of the slip table (including the mass of the moving parts of the servovalve–actuator system, namely the actuator piston and arm).

[‡] The convention adopted throughout the paper is that compression in the actuator arm corresponds to a positive actuator force $F_a(s)$.

Substituting the above expression for $F_a(s)$ into Equations (13) and (17) reduces them to

$$S'(s) = \frac{x_t(s)}{x_c(s)} = \frac{H_t(s)}{s^3[(Vm_t)/(4\beta A)][1 + B(s)] + s^2 m_t k_{le}[1 + B(s)] + sA} \tag{22}$$

$$H'(s) = \frac{x_t(s)}{x_d(s)} = \frac{S'(s)[(1/s)K_{int} + K_{pro} + s(K_{ff} + K_{der})]}{1 + S'(s)[(1/s)K_{int} + K_{pro} + sK_{der} - s^2(K_{dp}m_t/A)[1 + B(s)]]} \tag{23}$$

where the $(\,)'$ used for the transfer functions $S(s)$ and $H(s)$ indicates that they incorporate the effect of reaction mass flexibility (or foundation compliance). Substituting the expressions for $B(s)$ and $H'(s)$ in Equations (20) and (23) into Equation (19) gives a final expression for the table transfer function $T(s)$ under bare table condition.

Figure 5 compares the magnitude and phase of the table transfer function[†,‡] for a flexible and rigid foundation.[§] The dynamic characteristics of the flexible foundation for the Rice University shaking table [4, 5] ($\omega_b = 170$ rad/s corresponding to 27 Hz, and $\xi_b = 0.042$) are used in generating these transfer functions. Notice the peak and notch sequence and the notch only in the magnitude and phase, respectively, of the table transfer function in the neighborhood of the foundation natural frequency. The large peak in the magnitude of the table transfer function at about 70 Hz in Figure 5 is commonly referred to as the oil column peak. It is due to the resonance behavior of the SDOF system having for spring the oil column enclosed in the two actuator chambers and for mass that of the slip table, m_t, including actuator piston and arm. The oil column frequency is given by [4, 8]

$$f_{oil} = \frac{A}{\pi}\sqrt{\frac{\beta}{Vm_t}} = 69.3\,(\text{Hz})^{¶} \tag{24}$$

2.5. *Effects of payload on shaking table transfer function*

Ideally, the dynamic performance of a shaking table should not be significantly affected by the payloads or the weight/configuration of the test structure. However, in real situations when a test structure (or payload) of significant weight (relative to the mass of the table) is mounted on the table, the transfer function of the shaking table system is affected. The effect of the payload depends on its weight and dynamic characteristics. A very stiff payload affects the shaking table

[†] In Figure 5 and hereafter the magnitude and phase transfer functions of the table are plotted against the cyclic frequency parameter f (in Hertz). The expression for the table transfer function in terms of f is simply obtained by using the substitution $s = i2\pi f$ (where $i = \sqrt{-1}$) in the table transfer function expressed in terms of the Laplace parameter 's'.

[‡] In computing the table transfer function, the following values of the table parameters, corresponding to the Rice University shaking table, are used [4, 5]: table gain factor: $k_t = 5408\,\text{cm}^3/\text{V s}$ ($330\,\text{in}^3/\text{V s}$); leakage coefficient: $k'_{le} = 2.377 \times 10^{-7}\,\text{cm}^3/\text{MPa s}$ ($10^{-10}\,\text{in}^3/\text{psi s}$); effective oil bulk modulus: $\beta = 675.7\,\text{MPa}$ (98,000 psi); piston effective cross-sectional area: $A = 82.13\,\text{cm}^2$ ($12.73\,\text{in}^2$); volume of oil column in the actuator: $V = 1668.86\,\text{cm}^3$ ($101.84\,\text{in}^3$); mass of the slip table including actuator piston and arm (moving parts): $m_t = 576\,\text{kg}$ ($3.29\,\text{lbs s}^2/\text{in}$ corresponding to a table weight of 1270 lbs); reaction mass including servovalve–actuator system (fixed parts): $m_b = 40823\,\text{kg}$ ($233\,\text{lbs s}^2/\text{in}$ corresponding to a weight of 90,000 lbs). The three-stage servovalve transfer function with zero time delay in Equation (3) is used. The proportional control gain K_{pro} is set to 0.394 V/cm (1.0 V/in), while all other table control gains are set to zero.

[§] The rigid foundation model is obtained by taking a base transfer function $B(s)$ equal to zero.

[¶] An oil column frequency of 69.3 (Hz) is obtained for the parameters of the Rice University shaking table given earlier.

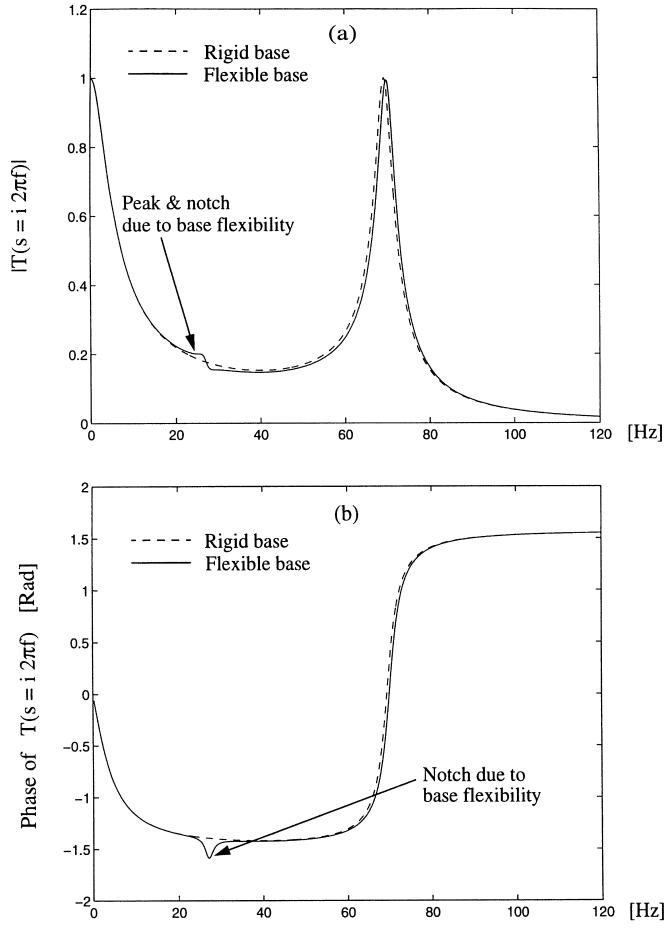

Figure 5. Effect of base flexibility on the shaking table transfer function for bare table condition: (a) magnitude of table transfer function with rigid and flexible base; (b) phase of table transfer function with rigid and flexible base.

system as if the mass of the slip table, m_t, were increased by the weight of the payload. On the other hand, a flexible payload affects the table transfer function in a much more complex way. In this second case, the table transfer function $T(s)$ in Equation (19) is modified in order to incorporate the effects that the total shear force $F_s(s)$ transmitted to the slip table by the flexible payload has upon (a) the servovalve–actuator transfer function $S(s)$, (b) the servo-hydraulic system transfer function $H(s)$, and (c) the base transfer function $B(s)$.[†] It is noted that only test

[†] The total shear force $F_s(s)$ transmitted by the payload to the slip table affects the base transfer function $B(s)$ through the force in the actuator $F_a(s)$.

structures modeled as linear elastic SDOF and two-dimensional MDOF systems are considered in this study.†

2.5.1. SDOF payload. First, we consider a payload acting as a single-degree-of-freedom (SDOF) system. From structural dynamics [9] it is known that the transfer function, hereafter referred to as payload transfer function, between the absolute displacement at the base of an SDOF system and its absolute (or total) displacement response has the following expression in Laplace notation‡

$$H_p(s) = \frac{x_{pa}(s)}{x_{ta}(s)} = \frac{x_{ta}(s) + x_p(s)}{x_{ta}(s)} = 1 + \frac{x_p(s)}{x_{ta}(s)} = \frac{s2\xi_p\omega_p + \omega_p^2}{s^2 + s2\xi_p\omega_p + \omega_p^2} \tag{25}$$

in which $x_{pa}(s)$ and $x_p(s)$ are the absolute and relative (to the slip table) displacements of the SDOF payload; $x_{ta}(s)$ is the absolute (or total) displacement of the slip table; ω_p and ξ_p are the undamped natural circular frequency and damping ratio, respectively, of the payload.

With reference to Figure 6(b), the total shear force (spring plus damping forces), $F_s(s)$, transmitted to the slip table by the SDOF payload is given by

$$F_s(s) = -s^2 m_p H_p(s)[x_{ta}(s)] \tag{26}$$

As shown in Figure 6(b), the total shear force transmitted by the payload to the slip table, $F_s(s)$, affects the motion of the reaction mass, as expressed by the following equation of dynamic equilibrium of the reaction mass:

$$s^2 m_b x_b(s) + s c_b x_b(s) + k_b x_b(s) = -s^2 m_t x_{ta}(s) + F_s(s) \tag{27}$$

where c_b and k_b denote the effective damping and stiffness coefficients, respectively, of the reaction or foundation mass.

Substituting the expression for $F_s(s)$ given in Equation (26) into Equation (27) and dividing throughout by $m_T = m_b + m_t$, we obtain the following expression for the base transfer function, which incorporates the effects of an SDOF payload as indicated by the subscript 'sdof'.

$$B_{sdof}(s) = \frac{x_b(s)}{x_t(s)} = \frac{-s^2(m_t/m_T)\{1 + (m_p/m_t)H_p(s)\}}{s^2\{1 + (m_p/m_T)H_p(s)\} + s2\xi_b\omega_b + \omega_b^2} \tag{28}$$

Figure 6(b) shows that in the presence of an SDOF payload, the force in the actuator, $F_a(s)$, becomes

$$F_a(s) = s^2 m_t x_{ta}(s) - F_s(s) \tag{29}$$

† The effects of test structures undergoing nonlinear inelastic deformations on the dynamic performance of the shaking table system are out of the scope of this study. Treatment of such effects would require a time domain simulation approach.

‡ Following the notation defined in Figure 6.

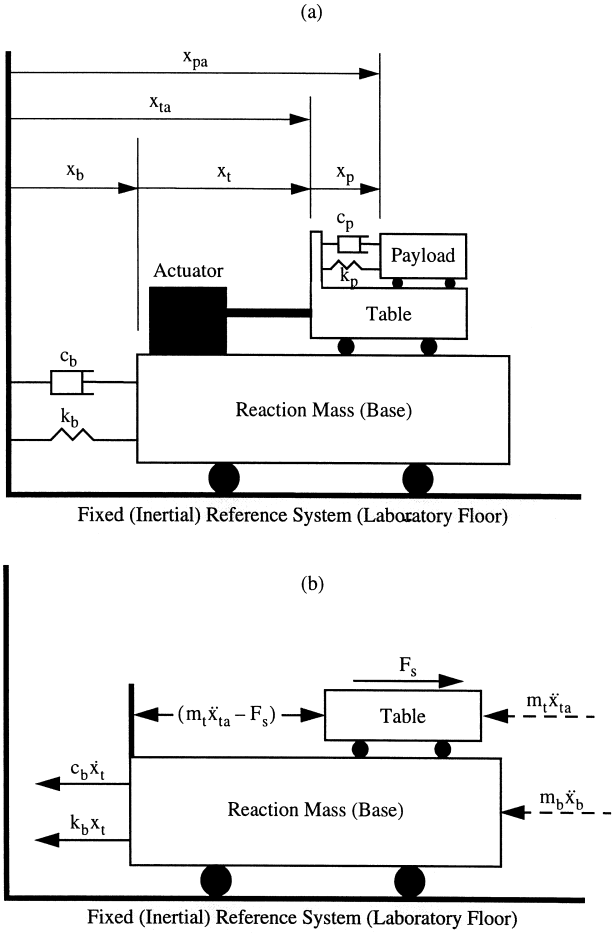

Figure 6. Shaking table with flexible base and SDOF payload: (a) Coordinate system; (b) Free body diagram.

Substituting the expression for $F_s(s)$ given in Equation (26) into Equation (29) and rearranging the terms, we obtain

$$F_a(s) = s^2[m_t + m_p H_p(s)]x_{ta}(s) = s^2 m_t x_t(s)\left[1 + \frac{x_b(s)}{x_t(s)}\right]\left[1 + \frac{m_p}{m_t}H_p(s)\right] \tag{30}$$

Then, recalling the definition $B_{sdof}(s) = x_b(s)/x_t(s)$, the following compact expression is obtained for $F_a(s)$:

$$F_a(s) = s^2 m_t x_t(s)[1 + B_{sdof}(s)]\left[1 + \frac{m_p}{m_t}H_p(s)\right] \tag{31}$$

For notational convenience, Equation (31) is rewritten as

$$F_a(s) = s^2 m_t x_t(s) H_{F1}(s) \tag{32}$$

where the operator $H_{F1}(s)$ is defined as

$$H_{F1}(s) = [1 + B_{sdof}(s)]\left[1 + \frac{m_p}{m_t} H_p(s)\right] \tag{33}$$

Substituting the expression for $F_a(s)$ in Equation (32) into Equations (13) and (17) reduces these two equations to

$$S'_{sdof}(s) = \frac{x_t(s)}{x_c(s)} = \frac{H_t(s)}{s^3(Vm_t/4\beta A)H_{F1}(s) + s^2 m_t k_{le} H_{F1}(s) + sA} \tag{34}$$

$$H'_{sdof}(s) = \frac{x_t(s)}{x_d(s)} = \frac{S'_{sdof}(s)[sK_{ff} + K_{pro} + (1/s)K_{int} + sK_{der}]}{1 + S'_{sdof}(s)[K_{pro} + (1/s)K_{int} + sK_{der} - K_{dp}(s^2 m_t/A)H_{F1}(s)]} \tag{35}$$

In the above equations, the $()'$ and $()_{sdof}$ indicate that the effects of foundation flexibility and SDOF payload are both accounted for.

The base and servo-hydraulic system transfer functions in Equations (28) and (35), respectively, are then used to obtain the following total shaking table transfer function, $T_{sdof}(s)$, which accounts for both foundation flexibility and the presence of an SDOF payload on the table:

$$T_{sdof}(s) = \frac{x_b(s) + x_t(s)}{x_d(s)} = \frac{x_t(s)}{x_d(t)}\left(\frac{x_b(s)}{x_t(s)} + 1\right) = H'_{sdof}(s)(B_{sdof}(s) + 1) \tag{36}$$

Figure 7 compares the magnitude and phase of the table transfer function for: (a) bare table condition, (b) a 408 kg (900 lbs) rigid payload, and (c) a 408 kg (900 lbs) SDOF payload.[†] It is observed that the flexible payload introduces a peak and notch distortion in the magnitude and a notch distortion in the phase of the table transfer function in the neighbourhood of the fixed base SDOF payload natural frequency. The table transfer functions in Figure 7 are obtained using the same table parameters as those used for the table transfer functions in Figure 5.

2.5.2. MDOF payload. To capture the dynamic behaviour of a shaking table loaded with a multi-degree-of-freedom (MDOF) payload, a new expression must be developed for the table transfer function $T(s)$. The present study considers a two-dimensional multi-storey frame-type test specimen as shown in Figure 8. As in the case of an SDOF payload, the total shear force transmitted by the payload to the table, $F_s(s)$, affects the force in the actuator arm $F_a(s)$, which in turn affects (a) the motion of the flexible foundation and thus the base transfer function $B(s)$, (b) the servovalve–actuator transfer function $S(s)$, and (c) the servo-hydraulic system transfer

[†] The dynamic characteristics of the 408 kg (900 lbs) payload modeled as an SDOF system with a fixed base natural frequency of 10 Hz are: $\omega_p = 62.8$ rad/s, $\xi_p = 0.02$ and $m_p = 408$ kg (2.33 lbs s^2/in).

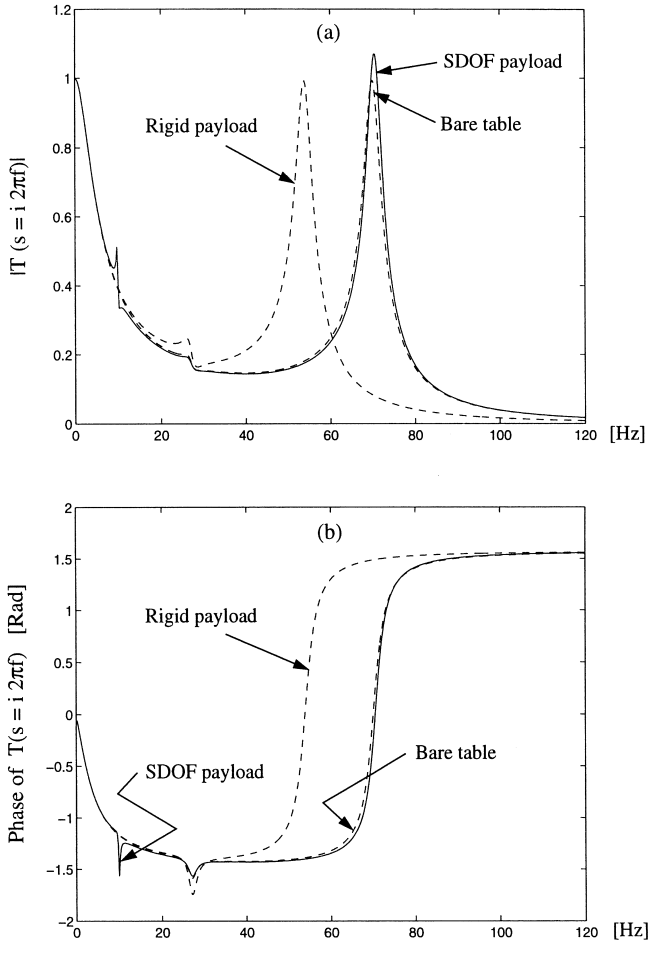

Figure 7. (a) Magnitude and (b) phase of table transfer function (including base flexibility) for (i) bare table condition, (ii) table loaded with a 408 kg (900 lbs) rigid payload, and (iii) table loaded with a 408 kg (900 lbs) SDOF payload.

function $H(s)$. Referring to the N-storey building frame model displayed in Figure 8, the equation of motion of the MDOF payload can be written in the usual matrix form

$$[m_p]\{\ddot{x}_p(t)\} + [c_p]\{\dot{x}_p(t)\} + [k_p]\{x_p(t)\} = -[m_p]\{1\}(\ddot{x}_b(t) + \ddot{x}_t(t)) \tag{37}$$

where

$$[m_p]_{(N\times N)} = \begin{bmatrix} m_{p,1} & \dots & 0 \\ \dots & \dots & \dots \\ 0 & \dots & m_{p,N} \end{bmatrix}$$ is the lumped mass matrix of the building model

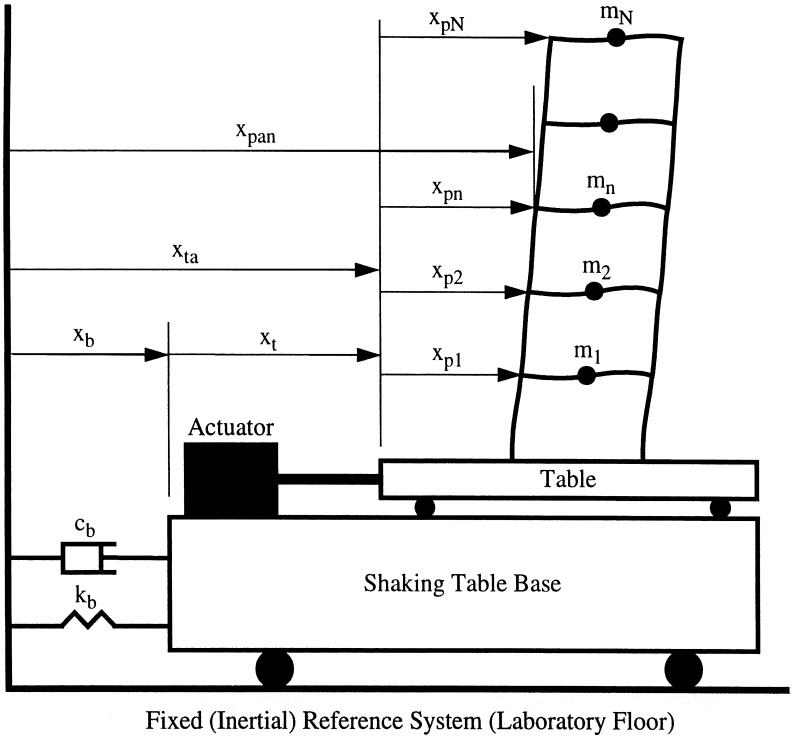

Figure 8. Table loaded with an MDOF payload: coordinate system.

$$[c_{\mathrm{p}}]_{(N\times N)} = \begin{bmatrix} c_{\mathrm{p},11} & \cdots & c_{\mathrm{p},1N} \\ \cdots & \cdots & \cdots \\ c_{\mathrm{p},N1} & \cdots & c_{\mathrm{p},NN} \end{bmatrix}$$ is the damping matrix of the building model

$$[k_{\mathrm{p}}]_{(N\times N)} = \begin{bmatrix} k_{\mathrm{p},11} & \cdots & k_{\mathrm{p},1N} \\ \cdots & \cdots & \cdots \\ k_{\mathrm{p},N1} & \cdots & k_{\mathrm{p},NN} \end{bmatrix}$$ is the (condensed) lateral stiffness matrix of the building model

$$\{x_{\mathrm{p}}(t)\}_{(N\times 1)} = \begin{bmatrix} x_{\mathrm{p}1} \\ \vdots \\ x_{\mathrm{p}N} \end{bmatrix}$$ is the vector of floor lateral displacements relative to the slip table (or base of the building model);

$$\{1\}_{(N\times 1)} = \begin{bmatrix} 1 \\ \vdots \\ 1 \end{bmatrix}$$ is an N-dimensional vector of unit load influence coefficients.

Assuming orthogonal (classical) damping and using mode superposition [9], it is possible to obtain the following expression, in Laplace domain, for the transfer function $\{H_{\mathrm{pm}}(s)\}$ between the absolute displacement at the base of the MDOF payload (which corresponds to the table absolute displacement $x_{\mathrm{ta}}(s)$) and the vector of floor lateral displacements relative to the table $\{x_{\mathrm{p}}(s)\}$

$$\{H_{\mathrm{pm}}(s)\} = \frac{\{x_{\mathrm{p}}(s)\}}{x_{\mathrm{ta}}(s)} = -\sum_{n=1}^{N} \{\phi_n\} \frac{\{\phi_n\}^{\mathrm{T}}[m_{\mathrm{p}}]\{1\}}{M_n} \frac{s^2}{s^2 + s2\xi_n\omega_n + \omega_n^2} \tag{38}$$

where

$\{\phi_n\} = \begin{bmatrix} \phi_{n1} \\ \phi_{n2} \\ \vdots \\ \phi_{nN} \end{bmatrix}$ is the nth undamped vibration mode shape of the test structure (under fixed base condition);

$[\Phi] = [\{\phi_1\}\ \{\phi_2\} \ldots \{\phi_n\}]$ is the modal matrix or matrix of undamped mode shapes;

$[M] = [\Phi]^{\mathrm{T}}[m_{\mathrm{p}}][\Phi]$ is the diagonal modal-coordinate generalized mass matrix;

$[C] = [\Phi]^{\mathrm{T}}[c_{\mathrm{p}}][\Phi]$ is the diagonal modal-coordinate generalized damping matrix;

$[K] = [\Phi]^{\mathrm{T}}[k_{\mathrm{p}}][\Phi]$ is the diagonal modal-coordinate generalized stiffness matrix;

M_n, C_n, and K_n are the nth diagonal elements of the modal-coordinate generalized mass, damping, and stiffness matrices $[M]$, $[C]$, and $[K]$, respectively; $\omega_n = (K_n/M_n)^{1/2}$ and $\xi_n = C_n/(2M_n\omega_n)$ are the undamped natural circular frequency and damping ratio, respectively, of the nth mode of vibration of the MDOF payload under fixed base condition.

The total base shear force (elastic + damping forces), $F_{\mathrm{s}}(s)$, transmitted by the flexible MDOF payload to the table can be obtained as the sum of all floor inertia forces[†] as

$$F_{\mathrm{s}}(s) = -s^2 \sum_{n=1}^{N} m_n x_{\mathrm{pan}}(s) = -s^2\{1\}^{\mathrm{T}}[m_{\mathrm{p}}]\{x_{\mathrm{pa}}(s)\} = -s^2\{1\}^{\mathrm{T}}[m_{\mathrm{p}}]\{\{x_{\mathrm{p}}(s)\} + \{1\}x_{\mathrm{ta}}(s)\} \tag{39}$$

in which $\{x_{\mathrm{pa}}(s)\}$ denotes the vector of floor absolute (or total) lateral displacements of the MDOF payload.[‡] Substituting the expression for $\{x_{\mathrm{p}}(s)\}$ given in Equation (38), namely $\{x_{\mathrm{p}}(s)\} = \{H_{\mathrm{pm}}(s)\}x_{\mathrm{ta}}(s)$, into the last term of Equation (39) yields the following expression for the total shear force $F_{\mathrm{s}}(s)$ transmitted to the table by the MDOF payload:

$$F_{\mathrm{s}}(s) = -s^2\{1\}^{\mathrm{T}}[m_{\mathrm{p}}](\{H_{\mathrm{pm}}(s)\} + \{1\})x_{\mathrm{ta}}(s) \tag{40}$$

[†] Inertia force of nth floor $= -m_n\ddot{x}_{\mathrm{pa},n}(t)$ or, in Laplace notation, $-s^2 m_{\mathrm{n}} x_{\mathrm{pa},n}(s)$.

[‡] $\{x_{\mathrm{pa}}(t)\} = x_{\mathrm{ta}}(t)\{1\} + \{x_{\mathrm{p}}(t)\}$.

For convenience of notation, Equation (40) is rewritten in the more compact form

$$F_s(s) = -s^2 H_{pml}(s) x_{ta}(s) \tag{41}$$

where the scalar operator $H_{pml}(s)$ is defined as

$$H_{pml}(s) = \{1\}^T [m_p](\{H_{pm}(s)\} + \{1\}) \tag{42}$$

Substituting the expression for the payload total shear force, $F_s(s)$, obtained in Equation (41) into the equation of dynamic equilibrium of the reaction mass, Equation (27), gives the following expression for the base transfer function $B(s)$:

$$B_{mdof}(s) = \frac{x_b(s)}{x_t(s)} = \frac{-s^2((m_t/m_T) + (H_{pml}(s)/m_T))}{s^2(1 + (1/m_T)H_{pml}(s)) + s2\xi_b\omega_b + \omega_b^2} \tag{43}$$

The subscript 'mdof' attached to the above base transfer function emphasizes that the latter incorporates the effects of an MDOF payload.

The total shear force $F_s(s)$ transmitted to the slip table by the MDOF payload also affects the value of the force in the actuator $F_a(s)$, which becomes

$$F_a(s) = s^2 m_t x_t(s) H_{F2}(s) \tag{44}$$

where the scalar operator $H_{F2}(s)$ is defined as

$$H_{F2}(s) = [1 + B_{mdof}(s)]\left[1 + \frac{H_{pml}(s)}{m_t}\right] \tag{45}$$

Substituting the expression for $F_a(s)$ given in Equation (44) into Equations (13) and (17) reduces these two equations to

$$S'_{mdof}(s) = \frac{x_t(s)}{x_c(s)} = \frac{H_t(s)}{s^3(Vm_t/4\beta A)H_{F2}(s) + s^2 m_t k_{le} H_{F2}(s) + sA} \tag{46}$$

$$H'_{mdof}(s) = \frac{x_t(s)}{x_d(s)} = \frac{S'_{mdof}(s)[sK_{ff} + K_{pro} + 1/sK_{int} + sK_{der}]}{1 + S'_{mdof}(s)[K_{pro} + (1/s)K_{int} + sK_{der} - (K_{dp}(s^2 m_t/A)H_{F2}(s)]} \tag{47}$$

In the above equations, the $()'$, and $()_{mdof}$ indicate that the effects of foundation flexibility and MDOF payload are both accounted for. Finally, the total shaking table transfer function, $T_{mdof}(s)$, for the shaking table loaded with an MDOF payload is obtained as

$$T_{mdof}(s) = \frac{x_b(s) + x_t(s)}{x_d(s)} = H'_{mdof}(s)(B_{mdof}(s) + 1) \tag{48}$$

Figure 9 compares the magnitude and phase of the table transfer function for (a) bare table condition and (b) a 408 kg (900 lbs) 3-DOF shear building payload. These table transfer functions

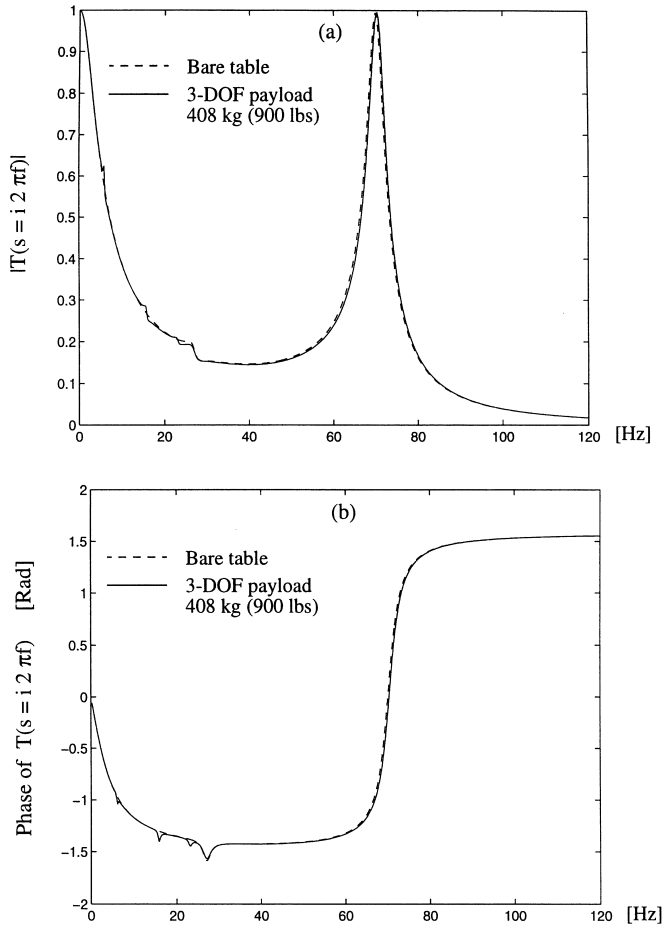

Figure 9. (a) Magnitude and (b) phase of table transfer function (including flexible base) for (i) bare table condition and (ii) table loaded with a 408 kg (900 lbs) 3-DOF payload.

were obtained using the table parameters defined earlier. The dynamic characteristics of the 3-DOF shear building payload are as follows:

Undamped natural circular frequencies:

$$\omega_1 = 37.52\left(\frac{\text{rad}}{\text{s}}\right), \quad \omega_2 = 99.55\left(\frac{\text{rad}}{\text{s}}\right), \quad \omega_3 = 145.54\left(\frac{\text{rad}}{\text{s}}\right)$$

Undamped vibration mode shapes:

$$\{\phi_1\} = \begin{bmatrix} 0.2928 \\ 0.5731 \\ 0.7654 \end{bmatrix}, \quad \{\phi_2\} = \begin{bmatrix} 0.6605 \\ 0.4576 \\ -0.5953 \end{bmatrix}, \quad \{\phi_3\} = \begin{bmatrix} 0.6914 \\ -0.6799 \\ 0.2446 \end{bmatrix}$$

Modal damping ratios: $\xi_1 = \xi_2 = \xi_3 = 0.02$
Floor masses: $m_1 = m_2 = m_3 = 136$ kg (0.7772 lbs s^2/in)
Storey lateral stiffnesses (from base to top):

$$k_1 = 1067.7 \text{ kN/m}, \quad k_2 = 915.2 \text{ kN/m}, \quad \text{and} \quad k_3 = 762.7 \text{ kN/m}$$
$$(6097 \text{ lbs/in}) \qquad (5226 \text{ lbs/in}) \qquad (4355 \text{ lbs/in})$$

We observe that: (a) the flexible MDOF payload produces a peak and notch distortion and only a notch distortion in the magnitude and phase, respectively, of the table transfer function near the three payload natural frequencies, (b) the present payload, which is realistic, affects only insignificantly both the frequency and amplitude of the oil column peak as compared to the bare table condition, and (c) the peak in the magnitude of the table transfer function due to foundation compliance is slightly reduced by the presence of the payload, mainly due to dynamic interaction with the third mode of vibration of the payload.

3. SENSITIVITY ANALYSIS OF SHAKING TABLE TRANSFER FUNCTION

Based on the shaking table transfer function developed herein from basic principles and well validated experimentally [4, 5], an in-depth sensitivity analysis was performed to investigate the effects and relative importance of the various parameters (control gain parameters, payload characteristics, and servovalve time delay) that affect the shaking table dynamics. The purpose of this sensitivity analysis is to identify the general performance trend of the shaking table system under a wide range of operating and payload conditions. Also in order to better capture (or enhance) the individual effects of the various parameters, this sensitivity analysis was performed using control gain settings that are different from those used for optimum shaking table performance.[†] Thus, the shaking table transfer function sensitivity analysis to control gain parameters is performed by increasing, starting from zero, the value of one control gain parameter at a time, while keeping the other control gain parameters at zero, expect for the proportional gain K_{pro}.[‡]

3.1. Sensitivity to table control gain parameters

In this section, we analyse the sensitivity of the total shaking table transfer function to the various control gain parameters (K_{pro}, K_{int}, K_{der}, K_{ff} and K_{dp}) using the analytical expression for the table transfer function $T(s)$ in Equation (19) for bare table condition, which accounts for the flexibility of the reaction mass.

[†] A forthcoming paper will present (a) a procedure for optimum shaking table tuning based on the analytical shaking table model developed herein and (b) a correlation study between analytical and experimental shaking table transfer functions for optimum control parameter settings corresponding to various payload conditions.

[‡] For meaningful shaking table response, the proportional gain must take a non-zero value. Thus, when the individual effects of the other control gain parameters were analyzed, the proportional gain K_{pro} was always kept equal to 0.394 V/cm (1.0 V/in).

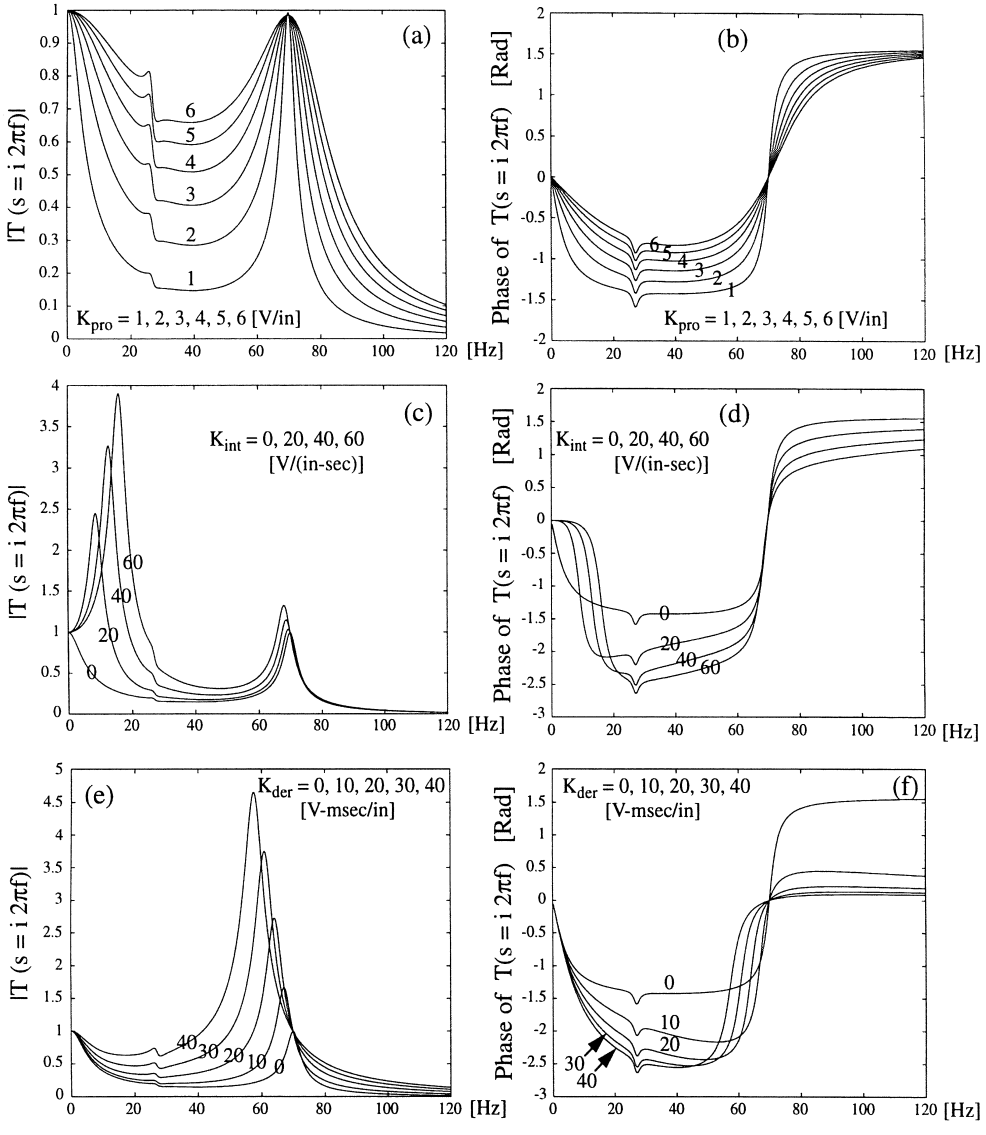

Figure 10. Effects of the PID control gains upon the shaking table transfer function for bare table condition: (a), (b): $K_{pro} = 0.39, 0.79, 1.18, 1.57, 1.97, 2.36$ V/cm (1, 2, 3, 4, 5, 6 V/in); (c), (d): $K_{int} = 0, 7.87, 15.75, 23.62$ V/cm s (0, 20, 40, 60 V/in s); (e), (f): $K_{der} = 0, 3.94, 7.87, 11.81, 15.75$ Vms/cm (0, 10, 20, 30, 40 Vms/in).

3.1.1. Sensitivity to PID control gains. Figure 10 shows the shaking table transfer function sensitivities to the PID gains. It is observed that the main effect of increasing the proportional gain, K_{pro}, is to raise the magnitude of the transfer function in the low and intermediate frequency range (from 0 to 60 Hz). An increase in the proportional gain also improves the phase transfer

function by reducing the phase shift in the low and intermediate frequency range. The inversion frequency,† which occurs at the oil column frequency, is not affected by the proportional gain. An increase in the integral gain, K_{int}, raises the magnitude of the table transfer function mainly in the low-frequency range (from 0 to 30 Hz) and improves the phase response of the table in the very low-frequency range (0–15 Hz). Increasing the derivative gain, K_{der}, has the main effect of increasing the amplitude of the oil column peak and simultaneously reducing the oil column frequency. An increase in K_{der} also raises the magnitude of the table transfer function in the intermediate frequency range (5–40 Hz). However, an increase in the derivative gain increases significantly the phase shift between table command and table response in the low and intermediate frequency range (5–50 Hz).

3.1.2. Sensitivity to feed-forward (FF) and differential pressure (ΔP) *control gains.* Figure 11 shows the sensitivities of the shaking table transfer function to the feed-forward, K_{ff}, and differential pressure, K_{dp}, gains. Observe that increasing K_{ff} heightens and widens the oil column peak, but improves dramatically the phase performance of the table in the low and intermediate frequency range. An increase in the delta pressure gain, K_{dp}, reduces the magnitude of the oil column peak without affecting the oil column frequency, thus explaining the common reference to the dP-gain as 'numerical damping'.

3.2. Sensitivity to payload characteristics

Two separate sensitivity analyses were performed: the first one to investigate the effects of a rigid payload of varying mass upon the total shaking table transfer function, and the second to investigate the effects of a flexible SDOF payload (which, for a given mass and damping ratio, is characterized by its natural vibration frequency). The control gain setting used to perform these sensitivity analyses ($K_{pro} = 0.394$ V/cm (1.0 V/in), $K_{int} = K_{der} = K_{ff} = K_{dP} = 0$) was chosen so as to enhance the payload effects on the table transfer function.

3.2.1. Sensitivity to rigid payload. Figures 12(a) and 12(b) show that an increase in the mass of the rigid payload (a) lowers the oil column frequency without affecting the amplitude of the oil column peak, (b) raises slightly the magnitude of the table transfer function in the intermediate frequency range (20–40 Hz), and (c) increases slightly the peak and the notch distortion (due to foundation compliance) in the magnitude and phase, respectively, of the table transfer function. Increasing the weight of the rigid payload also affects the phase of the table transfer function by lowering its inversion frequency which simply follows the lowering of the oil column frequency.

3.2.2. Sensitivity to flexible SDOF payloads. Figures 12(c) and 12(d) display a three-dimensional plot and corresponding contour plot, respectively, of the transfer function of the shaking table loaded with a 272 kg (600 lbs) SDOF payload of varying natural frequency and 5 per cent damping ratio. These plots show clearly the peak arising in the table transfer function in the vicinity of the payload natural frequency. With varying payload natural frequency, this peak follows approximately the 45° line between the frequency and payload natural frequency axes. It is also observed that when this line of resonant peaks intersects the oil column frequency region

† Frequency at which the phase of the transfer function changes sign.

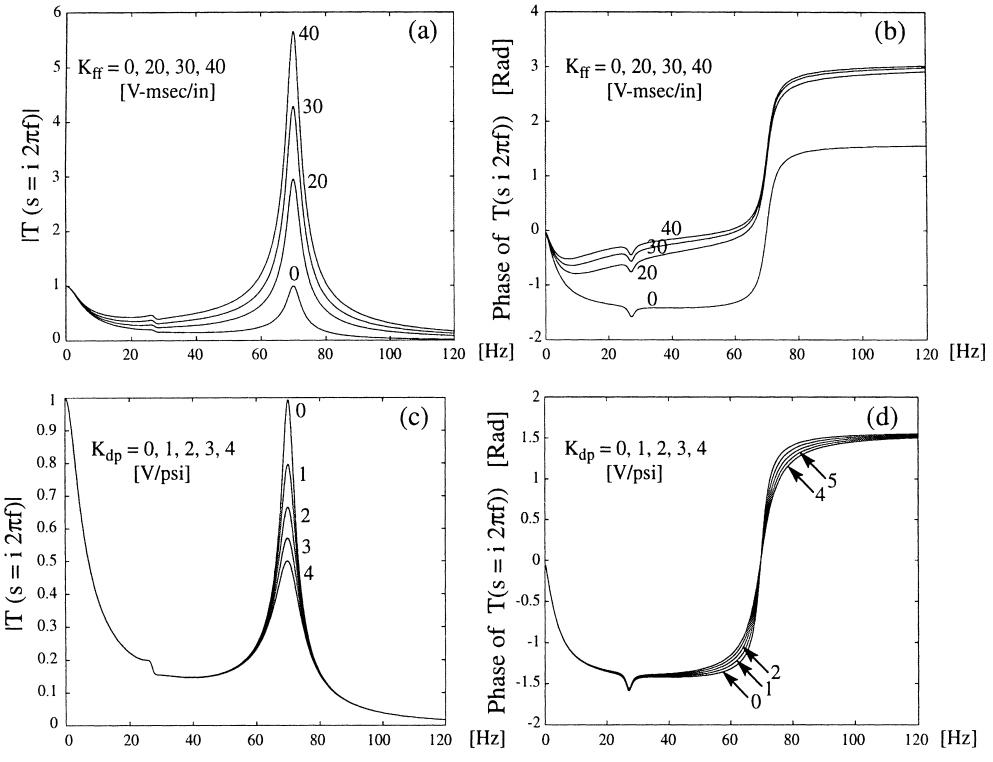

Figure 11. Effects of the feed-forward and differential pressure gains upon the shaking table transfer function for bare table condition: (a), (b): $K_{ff} = 0$, 7.87, 11.81, 15.75 Vms/cm (0, 20, 30, 40 Vms/in); (c), (d): $K_{dp} = 0$, 145.0, 290.1, 435.1, 580.1 V/MPa (0, 1, 2, 3, 4 V/psi).

(frequency band between 50 and 70 Hz), a strong dynamic interaction occurs between the payload and the oil column in the actuator giving rise to two very high peaks: one at a frequency lower than the oil column frequency for rigid payload condition and the other at a frequency higher than the oil column frequency for bare table condition.

Figures 12(e)–12(g) give a sequence of detailed cross-sections of the three-dimensional table transfer function of Figure 12(c). From Figure 12(e), it is observed that as the payload natural frequency increases starting from the low-frequency end, (a) the payload peak and notch increase in amplitude with the bottom of the notch located precisely at the payload natural frequency, and (b) the oil column peak increases and shifts to the right (i.e. apparent oil column frequency increases). Also note in Figure 12(e) the dynamic interaction between the payload with 30 Hz natural frequency and the flexible reaction mass which has a natural frequency around 27 Hz. For flexible payloads, the apparent oil column peak is very close to that for bare table condition as shown in Figure 12(e) for a payload with a natural frequency of 10 Hz. Although not shown here due to space limitation, it was found that for a given natural frequency, the payload peak and notch distortion increases in size for increasing payload weight. As the payload natural frequency continues to increase, (a) the payload peak increases dramatically as shown in Figure 12(f) for the

payload natural frequency of 45 Hz, and then decreases back, (b) with some 'frequency delay' relative to the payload peak, the apparent oil column peak also increases dramatically as shown in Figure 12(e) for the payload natural frequency of 55 Hz and decreases back as shown in

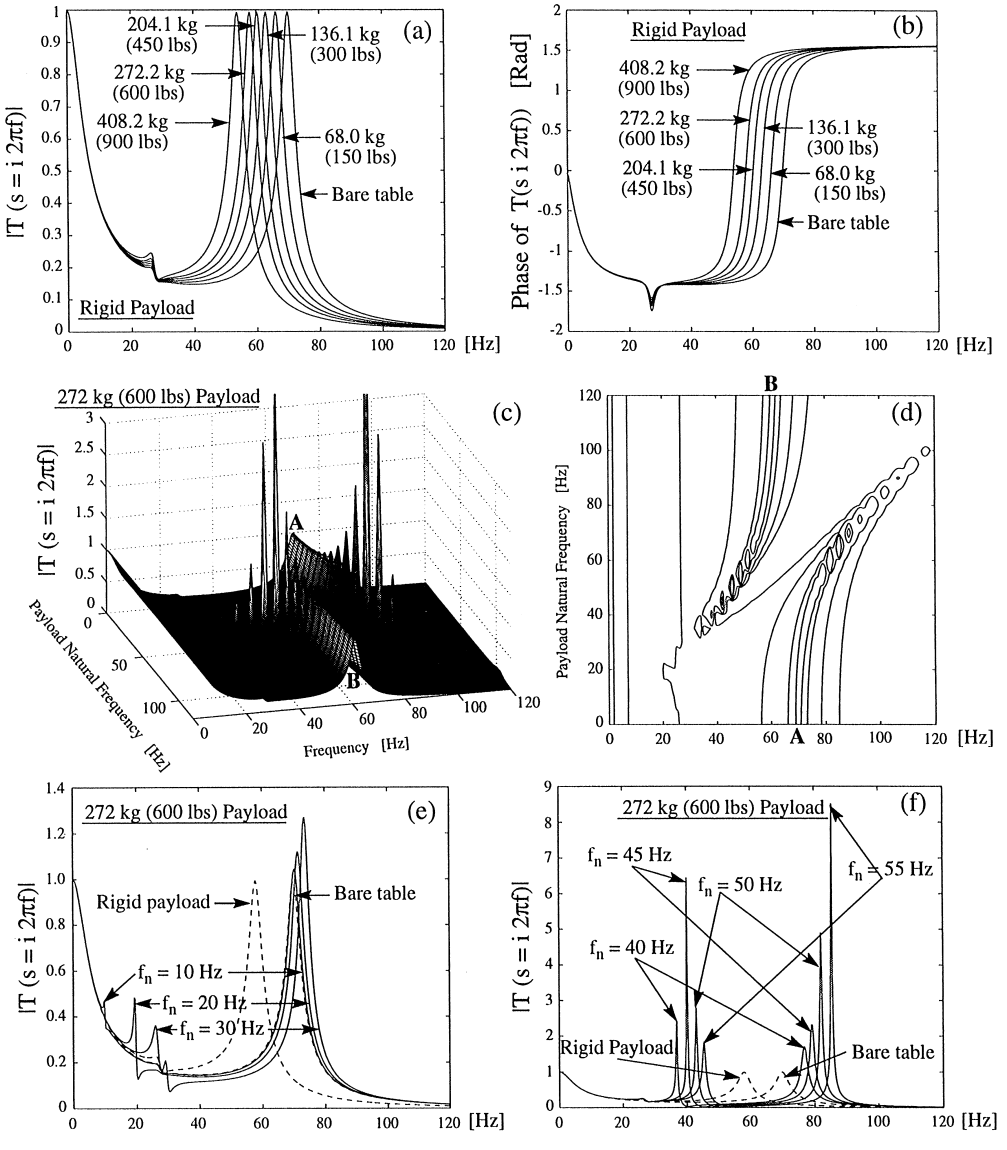

Figure 12. Effects of the payload upon the shaking table transfer function: (a), (b): Effect of rigid payload of increasing mass; (c), (d): 3D and contour plots of magnitude of table transfer function; (e), (f): Effect of 272 kg (600 lbs) SDOF payload of increasing natural frequency. Effects of payload upon the shaking table transfer function: (g) Effect of 272 kg (600 lbs) SDOF payload of increasing natural frequency; (h), (i): Limit cases: extremely stiff and extremely flexible 272 kg (600 lbs) SDOF payload.

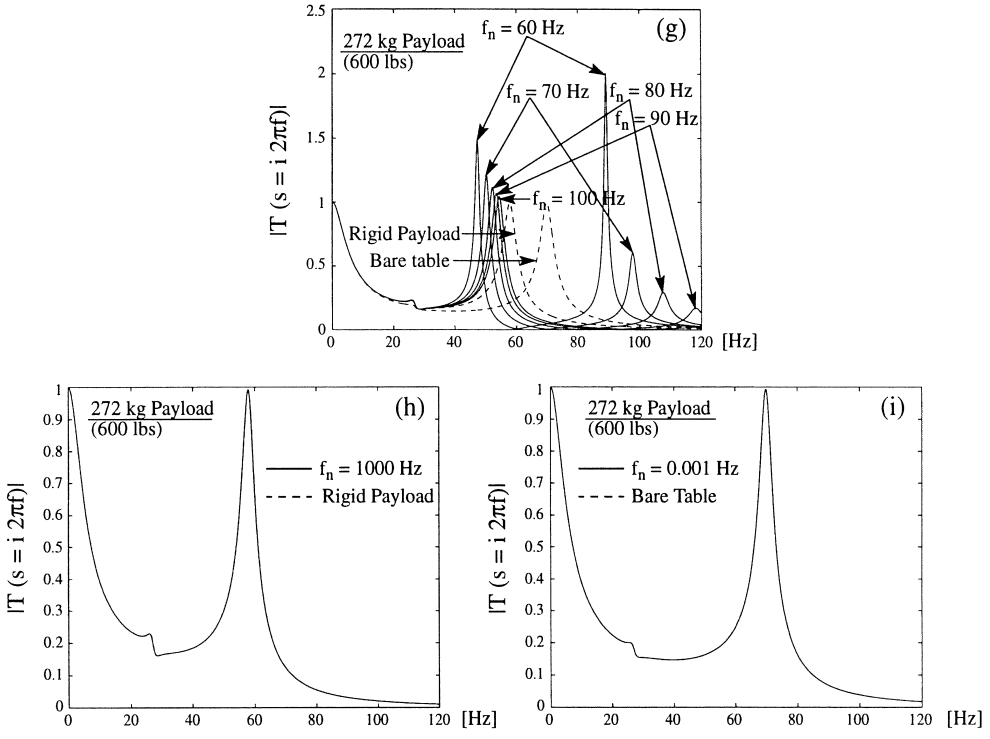

Figure 12. Continued.

Figure 12(g). Note in Figure 12(f) that the bottom of the now very wide payload notch is still located precisely at the payload natural frequency.

As the SDOF payload natural frequency keeps increasing beyond the oil column frequency for bare table condition (=69.3 Hz), both the payload peak and the apparent oil column peak decrease in size while their respective frequencies increase as shown in Figure 12(g). It is very interesting to observe from Figures 12(g) and (e) that with the payload natural frequency continuing to increase, the payload peak tends asymptotically to the apparent oil column peak for rigid payload condition. Thus, for high and increasing payload natural frequency, the former payload peak mutates progressively into the apparent oil column peak, while the former apparent oil column peak takes progressively the role of the payload peak. Note that at low payload natural frequency, the payload introduces a peak and notch sequence on the table transfer function, see Figure 12(e), while at high payload natural frequency, the notch precedes the peak, see Figure 12(g). But for any payload natural frequency, the bottom of the notch is located precisely at the payload natural frequency. Figures 12(h) and 12(i) show that the table transfer function developed tends to the correct limits, namely to the table transfer function for rigid payload as the payload becomes 'infinitely' stiff (here a payload natural frequency of 1000 Hz was considered), and to the table transfer function for bare table condition as the payload becomes 'infinitely' flexible (here a payload natural frequency of 0.001 Hz was considered). Very flexible

payloads 'decouple' from the shaking table in the sense that they do not affect the table transfer function (i.e. their presence is not felt by the shaking table).

3.2.3. Sensitivity to flexible MDOF payload. The numerical investigations performed using the shaking table model developed indicate that the effect upon the table transfer function of an MDOF shear-building-type payload[†] of realistic mass and stiffness properties can be approximated very well by that of an SDOF payload with natural frequency equal to the first modal frequency of the MDOF payload and mass equal to the effective modal mass[‡] of the first mode of the MDOF payload [4, 5].

3.3. Sensitivity to servovalve time delay

In this section, we analyse the effect (upon the shaking table transfer function for bare table condition) of the servovalve time delay τ introduced in the three-stage servovalve transfer function $H_t(s)$ in equation (6). This time delay in the response of the main stage servovalve spool to a given electrical signal was observed experimentally to be on the order of 0.01 s [4, 5] which motivated its inclusion in the dynamic shaking table model developed.[§] As shown in Figures 13(a)–13(f), the servovalve time delay τ can affect significantly both the amplitude and phase of the shaking table transfer function. As observed from these figures, the effects of the servovalve time delay do not follow a simple behavioral trend. Note that different values of τ can change both the amplitude and frequency of the oil column peak. Furthermore, large values of τ can produce sharp and high peaks in the very low frequency range, similar to those produced by the integral gain K_{int} of the PID table displacement controller as shown in Figure 10(c). Some of these very low frequency peaks were observed experimentally and could be explained only by the servovalve time delay [4, 5].

4. CONCLUSIONS

In this paper, a linear dynamic model for uni-axial, stroke-controlled servo-hydraulic shaking table systems is developed from basic principles and using a versatile modular formulation. The model consists of an analytical expression for the transfer function, called total shaking table transfer function, between the desired/commanded absolute table displacement (or acceleration) and the actual absolute table displacement (or acceleration). Compared to the previous work by other researchers on shaking table modelling, the present model has the advantage of incorporating, in closed-form, servovalve time delay, reaction mass or foundation compliance, and MDOF payload effects. The predictive capabilities and robustness of this shaking table model are substantiated by an in-depth experimental–analytical correlation study [4, 5] performed by the

[†] The shear building models considered have well-spaced natural vibration frequencies.

[‡] As defined by Chopra [9].

[§] Experimental–analytical correlation studies performed by the authors have shown that the servovalve time delay τ plays a fundamental role in the understanding of actual shaking table dynamics [4, 5]. In fact, without accounting properly for the servovalve time delay, only a qualitative interpretation of experimental shaking table results is possible through the analytical shaking table model developed here. On the other hand, the shaking table model incorporating the servovalve time delay proved capable to predict very well the observed shaking table dynamics (in terms of total shaking table transfer function).

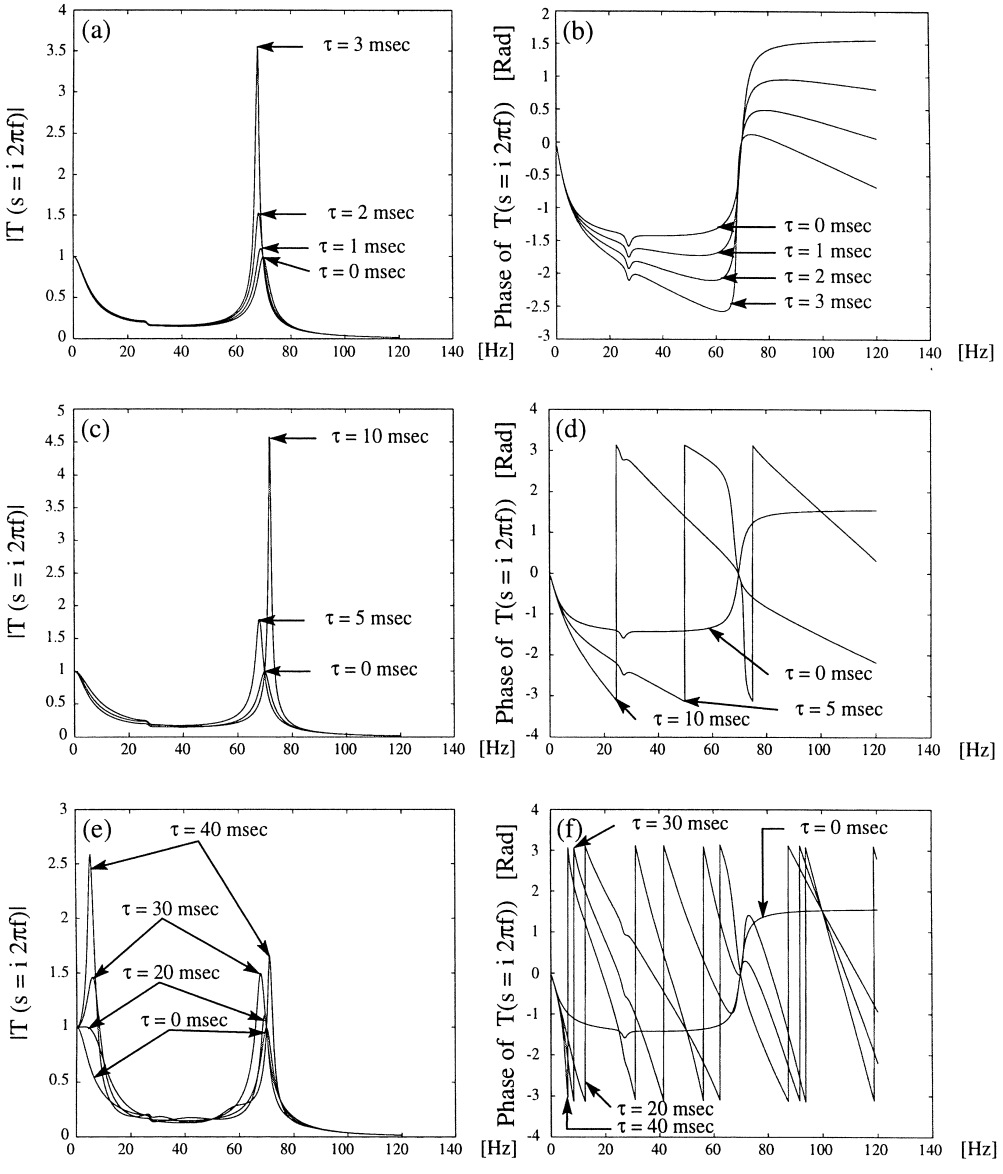

Figure 13. Effects of servovalve time delay 'τ' upon the shaking table transfer function for bare table condition.

authors based on the Rice University shaking table. This correlation study will be the object of a forthcoming paper.

The shaking table model developed, based on the characteristics of the Rice shaking table, is then used to perform a comprehensive sensitivity analysis of shaking table dynamics with respect

to (a) the proportional, integral, derivative, feed-forward, and differential pressure control gain parameters (of the displacement feedback table controller), (b) the payload dynamic characteristics, and (c) the servovalve time delay. The analytical sensitivity analysis with respect to SDOF payload natural frequency reveals a very interesting and complex dynamic interaction between the oil column in the actuator and the payload when the payload natural frequency approaches the oil column frequency. Understanding of this strong dynamic interaction is very important, especially for small shaking tables which require the use of small-scale test specimens with high natural frequencies. The sensitivity study also reveals that the servovalve time delay has a significant effect upon the total shaking table transfer-function.

In summary, the uni-axial, stroke-controlled, servo-hydraulic shaking table model presented in this paper is extremely useful in: (a) understanding the dynamics of a shaking table system and how it is influenced by control gain parameters, characteristics of the test structure, and base (or foundation) compliance; (b) guiding the optimal tuning of the table control gain parameters for a given test specimen and shaking table experiment; (c) designing shaking table experiments (i.e. pre-test simulation of experiments); (d) interpreting experimental shaking table results; and (e) formulating an efficient off-line control algorithm to control table acceleration with a displacement feedback controller. Furthermore, the model presented here provides a useful tool for designing new and upgrading existing servo-hydraulic shaking table systems of the type considered here.

By following the versatile, modular modelling approach used herein, the present uni-axial servo-hydraulic shaking table model can be further extended to include characteristics of other types of earthquake simulators [10] (e.g. digital control schemes, velocity/acceleration control systems, adaptive inverse control schemes, multi-axial tables, etc).

ACKNOWLEDGEMENTS

The support of the National Science Foundation under Grant No. BCS-9311031 and matching funds from Rice University for the design and construction of a small shaking table are gratefully acknowledged. The authors also wish to thank Prof. A. J. Durrani, Chairman of the Civil Engineering Department at Rice University, for his support and insightful suggestions provided in the course of this study.

REFERENCES

1. Rea D, Abedi-Hayati S, Takahashi Y. Dynamic analysis of electro-hydraulic shaking tables. *EERC Report No. 77/29,* Earthquake Engineering Research Center, University of California at Berkeley, CA, 1977.
2. Hwang JS, Chang KC, Lee GC. The system characteristics and performance of a shaking table. *NCEER Report No. 87-0004,* National Center for Earthquake Engineering Research, State University of New York at Buffalo, NY, 1987.
3. Rinawi AM, Clough RW. Shaking table-structure interaction. *EERC Report No. 91/13,* Earthquake Engineering Research Center, University of California at Berkeley, CA, 1991.
4. Trombetti TL. Experimental/analytical approaches to modeling, calibrating and optimizing shaking table dynamics for structural dynamic applications. *Ph.D. Dissertation*, Department of Civil Engineering, Rice University, Houston, TX, 1998.
5. Trombetti T, Conte JP, Durrani AJ. Correlation studies between analytical and experimental dynamic behavior of the Rice University shaking table. *Structural Research at Rice, Report No. 49,* Department of Civil Engineering, Rice University, December 1997.
6. Merritt HE. *Hydraulic Control Systems.* Wiley: New York, 1967.
7. Kuo BC. *Automatic Control Systems* (7th edn). Prentice-Hall: Englewood Cliffs, NJ, 1995.

8. Muhlenkamp M, Conte JP, Hudgings TR, Durrani AJ. Analysis, design, and construction of a shaking table facility. *Structural Research at Rice, Report No. 46,* Department of Civil Engineering, Rice University, Houston, TX, 1997.
9. Chopra AK. *Dynamics of Structures: Theory and Applications to Earthquake Engineering*. Prentice-Hall: New Jersey, 1995.
10. Filiatrault A, Kremmidas S, Seible F, Clark AJ, Nowak R, Thoen BK. Upgrade of first generation uniaxial seismic simulation system with second generation real-time three-variable digital control system. *Proceedings of the Twelfth World Conference on Earthquake Engineering*, Auckland, New Zealand, February 2000.
11. Trombetti T, Conte JP, Durrani AJ. Actuator-foundation-specimen interaction in a small shaking table. *Proceedings of 12th Engineering Mechanics Conference*, La Jolla, CA, 1998.

